Flow Behaviour of Ultrafine Cohesive Powder: View from Inside

Rostyslav Tykhoniuk and Jürgen Tomas
Otto von Guericke University of Magdeburg, Mechanical Process Engineering
P.O. Box 41 20, 39016 Magdeburg, Germany

Stefan Luding
Particle Technology, DelftChemTech, TU Delft,
Julianalaan 136, 2628 BL Delft, Netherlands

Michael Kappl and Hans-Jürgen Butt
Max-Planck-Institute for Polymer Research,
Ackermannweg 10, 55128, Mainz, Germany

Abstract Discrete element method (DEM) simulations will be presented with respect to modelling the standardised shear testers like Jenike shear cell or biaxial box. The main impact is made on modelling the flow behaviour of commercially widely used ultrafine cohesive powders (TiO_2, $CaCO_3$) and the influence of hysteretic contact models describing the microscopic particle-particle interaction behaviour with the load-dependent contact adhesion. The atomic force microscope (AFM)-based measurements of adhesion and friction forces between two particles are used to verify the contact behaviour on the micro-level. Therefore, the macroscopic dynamic behaviour of cohesive powder flow can be "microscopically" investigated and understood. Reference experiments with the Jenike shear cell coupled with volumetric strain measurements by triangulating laser displacement sensors will be shown and discussed as well. Comparison will be made between the simulations and experiments.

KEYWORDS: Particle, Discrete Element, Flow, Cohesion, Contact Model

I. INTRODUCTION

The well-known flow problems of cohesive particulate solids in storage and transportation containers, conveyors or process apparatuses include bridging, channelling, segregation, flooding, avalanching etc. In addition, the insufficient apparatus and system reliability of solid processing plants are also related to flow problems. Taking into account this list of selected technical problems and hazards, this motivates us to deal with the fundamentals of cohesive powder consolidation and flow behaviour, i.e. to develop a reasonable combination of particle and continuum mechanics. The goal of the present work is to build a numerical bridge between the microscopic particle properties based on the AFM measurements, theoretical models of elastic-plastic contact behaviour and the macroscopic powder flow behaviour of cohesive powders.

Continuum mechanical models and appropriate measuring methods were successfully applied to describe the flow behaviour of cohesive powders, as well as for practical design of process apparatus, e.g. silos. However, the essential constitutive functions of the powder "continuum" can be better described and understood with the help of particle mechanics [3]. The Discrete Element Method (DEM) [1] is an alternative solution, which allows us to take into account the contact and, what is especially important in our case, adhesion forces and introduce them into the equations of motion of the particles. By this sophisticated method, the dynamics of cohesive powders can be studied and understood „microscopically".

An interacting force between two macroscopic bodies can be measured by the spring balance method as a function of the elongation of the spring when they are separated. Reviews on AFM force measurements can be found at [20, 21]. Using the micron-sized particles glued to the end of an AFM cantilever as the force sensor, one can measure the adhesion and friction forces between the particles.

Combining the theoretical background and macroscopic shear tests of cohesive powders as well as the microscopic AFM measurements of the particle interaction forces, it becomes possible to develop an appropriate contact constitutive model to describe the deformation behaviour of ultrafine, cohesive frictional particles. In this context, to simulate efficiently the shear dynamics of cohesive powders the implementation of an irreversible inelastic contact flattening, which is an essential element and physical reason of the load-dependent increase of the adhesion force, is of vital importance. There exists a realistic and flexible microscopic model for contact laws with elastic, plastic, and adhesion forces, as based on macroscopic observations from bulk experiments [3, 4]. The model in a simplified form is applied to the Jenike shear test as well as biaxial shear box, in order to find out the relationships between the mechanical parameters of a single particle on a microscopic level and flow parameters of the powder continuum on the macroscopic level.

II. CONTACT FORCES BETWEEN SINGLE PARTICLES AND CONTACT CONSTITUTIVE MODELS

In terms of particle technology, powder processing and handling, the consolidation and non-rapid flow of dry, ultrafine and cohesive powders (particle diameter $d < 10 \, \mu m$) can be explained by the load -history dependent adhesion forces at particle contacts. Here we intend to focus on a characteristic, *soft* contact of two isotropic, *stiff*, linear elastic, smooth spherical particles. Thus, this soft or compliant contact displacement is assumed to be small $h_K/d << 1$ compared to the diameter of the stiff particle. The contact area consists of a representative number of molecules. Hence, continuum approaches are only used here to describe the force-displacement behaviour in terms of nanomechanics. The microscopic particle shape remains invariant during the dynamic stressing and contact deformation at this nanoscale. In powder processing, these particles are manufactured from uniform material in the bulk phase. These prerequisites are assumed to be suitable for the mechanics of dry particle contacts in many cases of industrial practice.

Here we will discuss in details the constitutive model of Luding used in the numerical simulations. We consider the contact of two isotropic and smooth spherical particles as the typical components of a particle packing under the static load F_N. Realistic and rather complicated contact model presented by Tomas [3] is very machine time spending to be implemented in the simulation software at present. That is why for the simulations we use the simplified contact law developed by Luding [5] (Fig. 1).
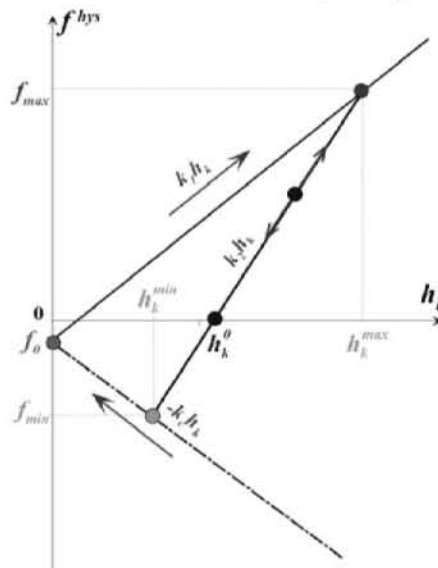

Fig. 1: Linearized normal force – displacement law for the DEM simulations [5]

At the point-contact moment, i.e. when the contact deformation or particle-particle overlap is equal to 0, interaction between the particles starts from a predefined adhesion level ($-f_0$, here attractive forces negative). The normal force then goes along the linear plastic yield limit with stiffness k_1, that takes care of a "perfect" plastic repulsion. Elastic deformation at the contact level is added by a linear spring, with a larger stiffness k_2 for unloading and reloading, so that the stiffness increases. This plastic loading and elastic unloading take care of velocity independent energy dissipation during contact; a linear dashpot is also considered that accounts for velocity proportional dissipation. The variable adhesion force (or cohesion on a microlevel) between the particles comes into the model by a "cohesive stiffness" k_c, which allows for changing the attractive forces up to a maximal attractive force f_{min} (per absolute value). One should notice also the force equilibrium state at a non-zero contact deformation of h_k^0. Cast into an equation, the normal force on particle is:

$$f_n^{hys} = \begin{cases} k_1 h_k - f_0 & \text{for loading} \\ k_2\left(h_k - h_k^0\right) & \text{for un-/reloading} \\ -k_c h_k - f_0 & \text{for unloading} \end{cases} \qquad (1)$$

The tangential force involves dissipation due to Coulomb friction, but also some tangential elasticity that allows for stick-slip behaviour on the contact level.

III. DIRECT MEASUREMENT OF ADHESION FORCES BETWEEN THE PARTICLES
Principle of direct force displacement measurement

The basics of the colloidal probe technique, or, in other words, direct assessment to the particle-particle or particle-surface interaction forces is the atomic force microscope. Using a micron-sized particle glued to the end of an AFM cantilever as the force sensor, this technique is developed for the study of colloidal interactions [12]. When comparing measured force-distance profiles between an AFM tip and a surface to theoretical models one encounters the problem of the poorly defined geometry of the AFM tip. An approach to get a better defined geometry has been demonstrated by Hüttl et al. [16]. They etched silicon AFM tips in an oven in the presence of oxygen and obtained tips with a spherical end of defined radius. A more universal solution is replacing the tip by a colloidal particle of well defined spherical shape, as shown in Fig. 2a.
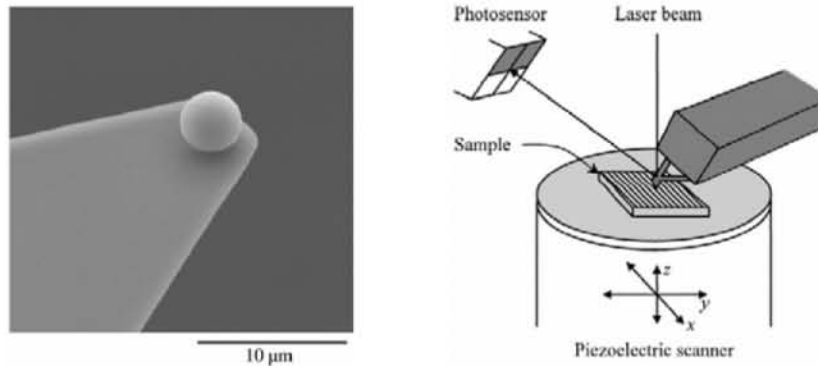

Fig. 2: **a)** Scanning electron micrograph of silanized silica microsphere glued to the end of a tipless atomic force microscope cantilever [12] and **b)** principle of an AFM. The sample is mounted onto a piezoelectric scanner and can be raster -scanned while in contact with the sharp tip that sits at the end of a cantilever. The deflection of the cantilever is detected with an optical lever technique. Therefore, a laser beam is reflected from the backside of the cantilever onto a split photodiode, and the change in position of the laser spot is recorded.

This so-called "colloidal probe technique" was first applied by Ducker et al. [17, 18] and Butt [19] and since then it has become a well established and powerful tool for the study of surface forces. Its measuring principle predestines it for the investigation of particle interaction, making single particle experiments feasible. The accessible range of particle size is typically limited to a range between 1 µm and 50 µm.

The measuring principle of the colloidal probe technique is identical to that of a standard AFM as outlined in Fig. 2b. In a force measurement the sample is moved up and down by applying a voltage to the piezoelectric translator, onto which the sample is mounted, while recording the cantilever deflection. The deflection of the cantilever is normally measured using the optical lever technique. Therefore a beam from a laser diode is focused onto the end of the cantilever and the position of the reflected beam is monitored by a position sensitive detector. The backside of the cantilever is usually covered with a thin gold layer to enhance its reflectivity. When a force is applied to the probe, the cantilever bends and the reflected light-beam moves on the detector.

The direct result of such a force measurement is the detector signal in volts, ΔV, versus the position of the piezo Δz_p, normal to the surface (Fig. 3a). To obtain a force-versus-distance curve, ΔV and Δz_p have to be converted into force and distance. To calculate the cantilever deflection from the detector signal, the corresponding conversion factor is needed which can be obtained from a linear fit of the "constant compliance" region. The tip-sample separation is then obtained by adding the cantilever deflection to the piezo position. The force, acting on the cantilever, F, is obtained by multiplying its deflection with its spring constant of the cantilever (Fig. 3b).
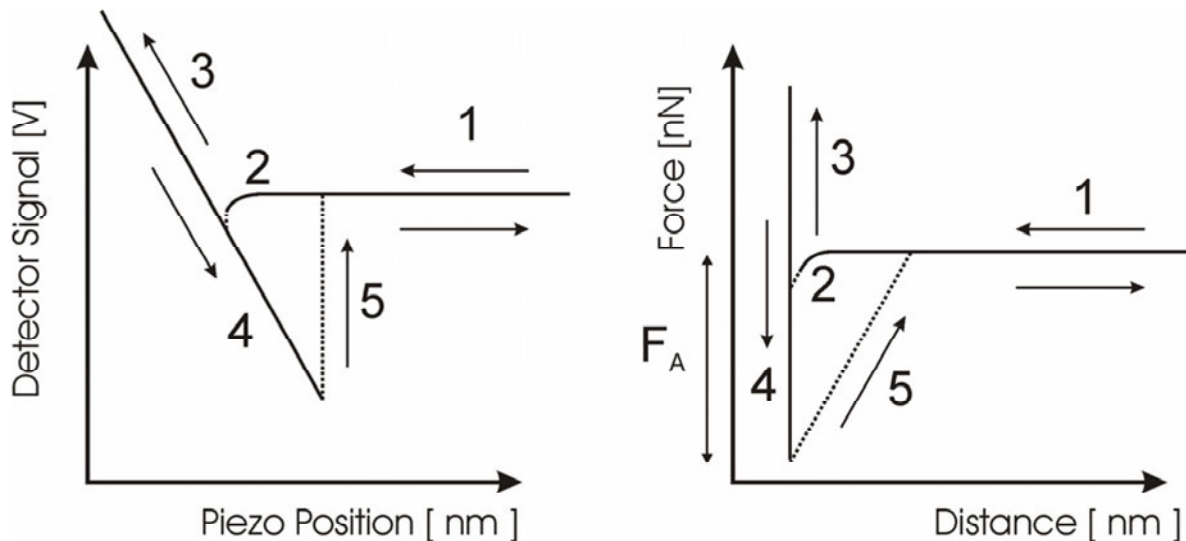

Fig. 3: a) Schematic of a deflection signal versus piezo position curve. When the colloidal probe is approaching but still far from the surface, no deflection will occur (1). When the probe gets close to the substrate, the (in this case attractive) surfaces forces will cause a bending of the cantilever towards the surface (2). As soon as the attractive force gradient becomes larger than the spring constant of the cantilever, the probe jumps in contact with the surface. From this moment, probe and surface will move in parallel (assuming no deformations of the surfaces occur). The resulting straight line corresponds to the so called "constant compliance" region (3). Upon retracting the sample, the probe will usually adhere to the surface, causing the cantilever to bend downwards (4). Eventually the bending force will become larger than the adhesion or pull-off force, and the cantilever will snap off the surface into its equilibrium position (5). b) Corresponding force versus distance curve after multiplying the deflection with the calibration coefficient obtained from a linear fit of the cantilever, and adding the cantilever deflection to the piezo position. F_A denotes the adhesion force.

Adhesion and friction force measurements

The adhesion between surfaces is governed by the deformation of the two bodies in contact, and the surface forces acting between them. These two phenomena are inherently coupled as the deformation will depend on the acting forces and at the same time the surface forces will depend on the resulting geometry of the bodies. This interdependence makes the theory of adhesion a complex problem that is still under debate.
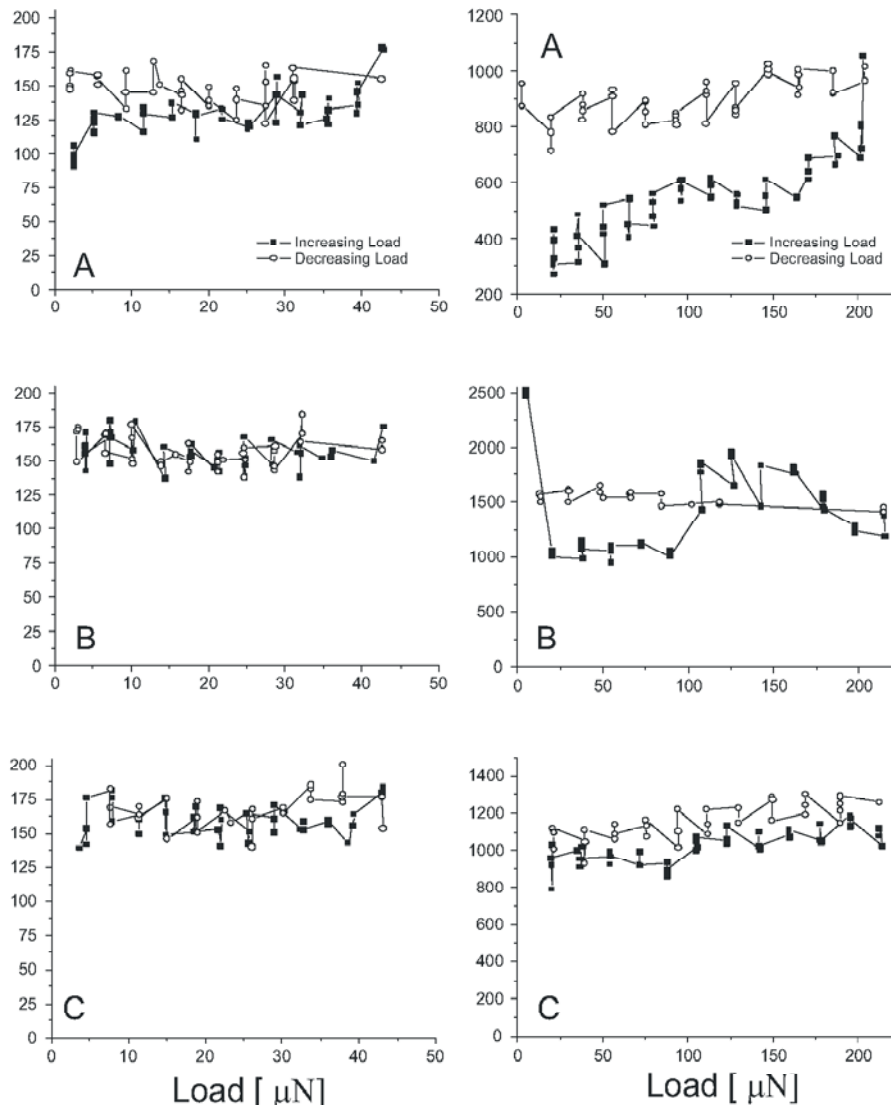

Fig. 4: Adhesion forces between two particles and a silicon wafer versus applied load. Plots A show the first cycle for each particle, where the load was increased stepwise to the maximum value and then decreased stepwise. An increase of the loading force from 2.5 to 43 μN for the first particle (left, R = 3.0 μm) leads to an increase in adhesion of about 50%. For the second particle (right, R = 8.3 μm) adhesion increased by 160%, while the load was increased from 21 μN to 204 μN. In subsequent cycles B and C, the load had no significant/systematic influence on the adhesion force, indicating plastic deformation of the particle.

In Fig. 4 the relation between adhesion force and loading force is plotted for two different particles which were mounted on cantilevers with spring constants of 3.8 N/m (left) and 18.6 N/m (right), respectively. In each of the six plots a series of adhesion force

measurements at the same spot on the silicon wafer are shown, where the load was first increased (full squares) and then decreased (open circles). Data in the plots denoted with A are from the first series of force curves with the corresponding particle, plots B and C are from consecutive series taken at other spots on the silicon wafer, but from the same spot on the particle. For the softer cantilever, an increase of about 50% in adhesion is obs erved (plot A, left) when the loading force is increased by a factor of 17, from 2.5 to 43 μN and this increased adhesion level remains even when the loading force is reduced again. In the subsequent series (plots B and C, left) the adhesion does not change any more. For the stiffer cantilever, that allowed higher loading forces, adhesion increased by about 160% during the first cycle when increasing the loading force by a factor of 10, from 21 to 204 μN (plot A, right). For the third series (plot C, right) no significant change in adhesion with load is observed and the value is about the same as the maximum reached during the first series. The second series (plot B, right) with this particle shows strong fluctuations, which may indicate a waver-surface irregularity at this spot.

IV. SIMULATIONS

One possibility to gain insight about the material behaviour of a granular packing is to perform elementary tests in the laboratory. Here, we chose as alternative the simulation with the discrete element model [6, 7, 8, 9, 10].

The discrete (or distinct) element solution sc heme assumes each of its constituents as the separate entity. Mechanical behaviour of a system, containing of, in general, randomly shaped particles can be simulated by a generalized particle flow model. The particles in this type of model have a rather independent behaviour. They displace independently from each other and interact only at contacts or interfaces (walls) between each of them. If the particles are assumed to be rigid, and the behaviour of the contacts is characterized using a soft contact approach, then the mechanical behaviour of such a system is described in terms of the movement of each particle and the inter -particle forces acting at each contact point. Newton's laws of motion for the translational and rotational degrees of freedom give the fundamental relationship between particle motion and the forces that induce them:

$$m_i \frac{d^2}{dt^2} \vec{r}_i = \vec{f}_i + m_i \vec{g} \qquad and \qquad I_i \frac{d}{dt} \vec{\omega}_i = \vec{t}_i \qquad\qquad (2),$$

with the gravitational acceleration $\vec{g}$, mass m_i of the particle, its position $\vec{r}_i$, the total force $\vec{f}_i$, acting on it due to contacts with other particles or with the walls, its moment of inertia I_i, its angular velocity $\vec{\omega}_i$, and the total torque $\vec{t}_i$.

Translational Shear Cell

The classical translational shear cell, developed by Jenike ([2]), is modelled (Fig. 5). Considering a suitable CPU-time for a certai n number of particles one should imagine that we simulate here only a small two-dimensional (2D) element from the real shear cell. Fig. 5 shows the model for 2000 titanium dioxide particles with diameter of about (3±0.5) μm. The upper wall (shear lid) is stress controlled, i.e. when the reaction force F_N changes because of the particle reorganization, the height of the shear lid is changed as well. The predefined normal stress $\sigma = F_N/A$ (A is replaced by d_Z in the 2D case). The horizontal shear rate of the upper part of the cell is preset, i.e. the upper ring is strain driven. As the direct response, the corresponding values of the reaction force are obtained, which acts on the lateral walls. Furthermore, the corresponding shear stresses $\tau = F_S/A$ are calculated enabling in this way to find the flow parameters of the simulated model powder. The shear

rate applied here is about 1-4 mm/min (similar to the one used in the Jenike shear cell in laboratory tests).
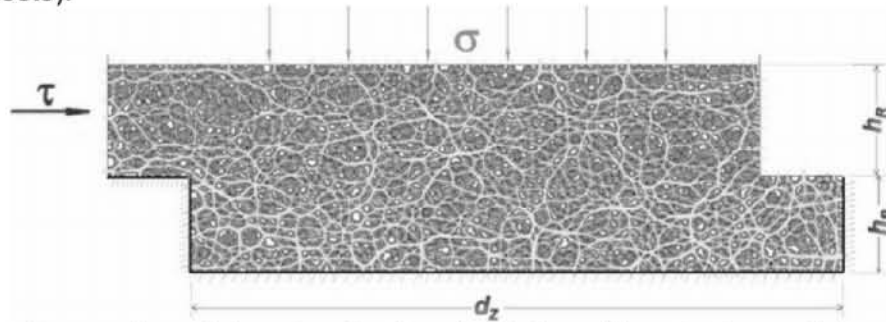

Fig. 5: The shear cell model system for the simulations (lines in the particle system show the initial contact forces, with line thickness proportional to force)

The first simulations are performed only with the linear adhesion contact law, which was implemented by the software (PFC2D, Itasca Inc.). For convenience, a constant adhesion force of 1-10 mN (0.1-1% of average contact forces of loading) was used to approximate the load-history dependent pull-off force [3]. Then a series of simulations is done applying the more general dissipative contact model for adhesive particles (Fig. 1), and the comparison is made.

Fig. 6 shows the force network during the shearing. The force lines run mostly from the upper left wall, where the shear force acts, to the lower right wall, where the corresponding resisting force acts. This correlates also sufficiently with the fact, that the orientation of the major principal stress σ_1 is just as tilted in the shear direction.
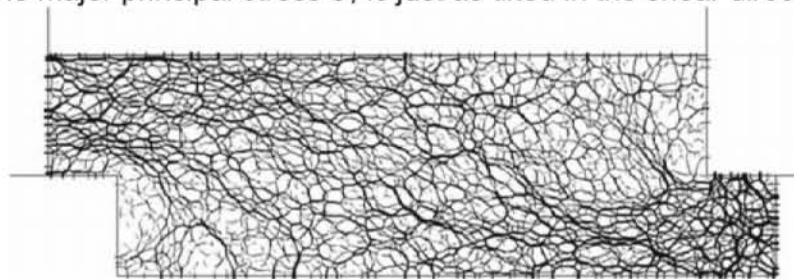

Fig. 6: Force distribution at the maximum value of shear stress
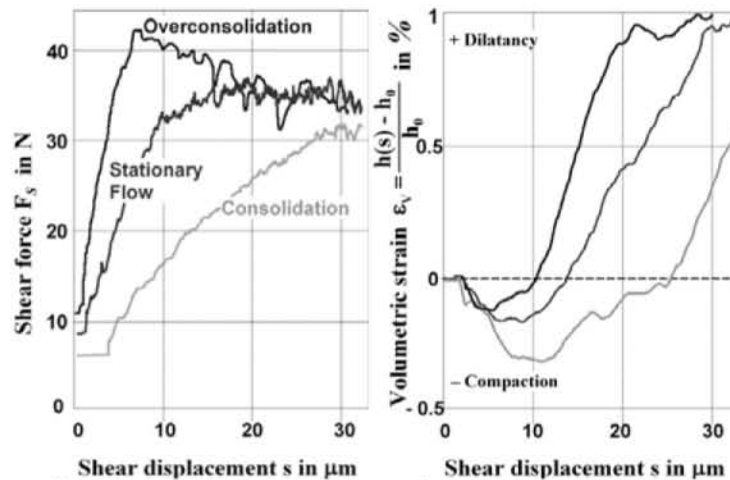

Fig. 7: Left: force-displacement diagram (steady-state flow) Right: volumetric strain for three different initial porosity values

Fig. 7 shows the force-displacement diagram (left) and the volumetric strain (right) at the constant normal stress of $\sigma_N=3\ kPa$ for three different values of porosity $\varepsilon=1-\rho_b/\rho_s$

(where ρ_b is the bulk material density, and ρ_s – the solid density), i.e. three so-called preshear tests. The upper curves in both graphs are obtained at a two-dimensional porosity of the particle system of $\varepsilon_{2D}=0.16$ (it corresponds appr. $\varepsilon_{3D}=0.46$ for three dimensions [11]). The typical behaviour of the overconsolidated powder is observed in this case achieving the peak force value along with the first-stage compaction at the beginning and tending to the steady state flow later on. The middle curves at $\varepsilon_{2D}=0.18$ ($\varepsilon_{3D}\sim0.50$) show almost ideal steady-state flow with the remark that the volumetric strain is coming to relatively stable state only at the end of the shear process, which does not come into agreement with the theoretical expectations. However, new measurements of the vertical movement of the shear lid (volumetric strain) performed with the real Jenike shear cell show the same tendency. The fluctuations of the shear force can be explained by means of the temporary and local shear-thickening and shear-thinning processes. The lower curves correspond to $\varepsilon_{2D}=0.20$ ($\varepsilon_{3D}\sim0.54$) and show the tendency of an underconsolidated powder. Taking into account the shear testing experiences, the good qualitative agreement is reached between the simulation results and the laboratory tests.
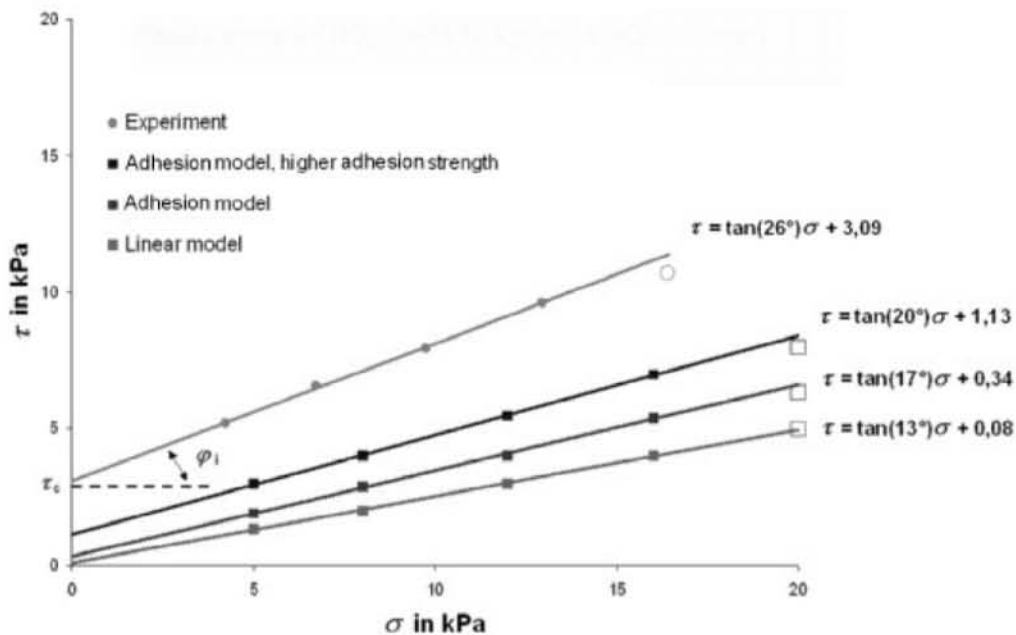

Fig. 8: Shear stress - normal stress diagram of yield locus 4 of model material (TiO_2, $\rho=3870$ kg/m^3, $v_s=2$ mm/min) for experiment and different microscopic force-displacement laws (linear and "cohesive")

Using the *steady-state shear stresses* for different applied normal stresses, as obtained from the Jenike cell experiments and simulations, the yield locus is defined. The slope of the yield locus gives the angle of internal friction of the material and the intersection with the vertical axis the macroscopic cohesion in stress units. Fig. 8 shows the comparison of the yield locus calculated from the Jenike shear cell experiments with the simulated yield loci obtained applying different contact laws with somewhat different parameters. The experimental line (the upper line) shows the internal friction angle of the powder "continuum" to be equal to $\varphi_i = 26°$, and the cohesion $\tau_c = 3.09$ kPa. The lowermost line is the result of the simulated shear test, where the simplest microscopic interaction between the particles was used, the linear-spring-dashpot contact model in normal direction, extended only by the constant adhesion force between the particles in contact $f_0 = 10$ mN, see Fig. 1. The preshear normal stress was $\sigma_{pre}=20$ kPa and, for the shear process, the adhesion force values f_0 were taken proportional to the reduced

macroscopic normal stresses. The average contact forces during preshear were in the range of 200-500 mN. The centre two lines are obtained using the elastic-plastic contact model with variable adhesion, Fig. 1, with $k_1 = 10^8$ N/m, $k_2 = 2k_1$, and the "microscopic adhesion stiffness" $k_c = k_2$ (lower curve) $k_c = 4k_2$ (higher curve), see Eq. 1, the latter leading to the macroscopic result for the internal friction angle $\varphi_i = 20°$, and the cohesion $\tau_c = 1.13$ kPa. Thus, comparison of the simulated data with experiments does not yet yield satisfactory quantitative agreement. However, the implemented "adhesion" contact model shows a "positive" influence on the macroscopic flow behaviour of a consolidated powder bed, when compared to the oversimplified linear contact model with load independent adhesion.

Together with another result ([5], [9], [10]), the fact that the macroscopic cohesion τ_c can be related to the maximal microscopic attractive force f_{min}, one can at least predict that the simulations should use about three times larger typical adhesion forces. Note that (due to the contact model) this has to be achieved by using smaller ratios k_1/k_2 – increasing k_c further does not lead to stronger adhesion. More systematic studies in this direction are in progress.

V. SUMMARY AND CONCLUSIONS

In summary, a set of DEM simulations based on different contact constitutive models was presented, and several macroscopic material parameters like, e.g., the friction angle, were extracted from the simulation data with cohesion (no friction) and with friction (no cohesion). Experimental set-up concerning the microscopic measurements of particle interactions based on AFM is presented as well as the one in part of macroscopic shear tests of bulk materials. Altogether this is a first step of a micro-modelling approach for cohesive frictional powders by means of going the whole long way from a measurement of ultra-fine single particles and implementing the complex microscopic contact constitutive laws for the contacts between the particles up to the shear dynamics of big particle systems finding out in this way the macroscopic flow parameters of bulk materials.

So far, good qualitative agreement of the simulations with experiments is reached. The implemented "cohesive" contact model shows a "positive" influence on the macroscopic flow behaviour of a consolidated powder bed. The model shows to be capable of simulating the cohesive properties of a material with variable adhesion (pull-off) force depending among others on the preconsolidation history of every inelastic particle contact deformation. An important result is the fact that the macroscopic cohesion can be related to the maximal microscopic attractive force.

Further material parameters have to be identified, and also the role of particle rotations is an open issue, as related to micro-polar constitutive models. In both simulations and experiments, rotations are active in the shear band where the rotational degree of freedom is activated. The corresponding parameter identification and the micro - macro-transition for anisotropic micro-polar continuum models is challenge for the future, like the implementation and simulation of experimentally determined force-laws [15] in three-dimensional systems.

VI. ACKNOWLEDGEMENT

VII. REFERENCES

[1]   Cundall, P. A, Hart, R. D.: Numerical modelling of diskontinua. 1st US Conference on DEM, Eng. Comput. 9, 101-113 (1992).

[2]   Jenike, A.W.: Storage and flow of solids, Eng. Exp. Station, Bull. No. 123, Univ. Utah, 1964.

[3]   Tomas, J.: Assessment of mechanical properties of cohesive particulate solids – part 1: particle contact constitutive model, Particulate Science & Technology 19 (2001) 2, 95-110.

[4]   Tomas, J.: in: K.L. Mittal, Particles on Surfaces 8: Detection, Adhesion and Removal, VSP Utrecht, 183-229, 2003.

[5]   Luding, S., Tykhoniuk, R., Tomas, J., Anisotropic material behaviour in dense, cohesive powders, CET (Chemical Engineering Technology) 26 (12), 1229-1232, 2003.

[6]   D'Addetta, G. A., Kun, F., Ramm, E.: On the application of a discrete model to the fracture process of cohesive granular materials, Granular Matter 4 (2), 77-90 2002.

[7]   Oda, M., Iwashita, K.: Study on couple stress and shear band development in granular media based on numerical simulation analyses, Int. J. of Enginering Science 38, 1713-1740, 2000.

[8]   Kruyt, N. P., Rothenburg, L.: Statistics of the elastic behaviour of granular materials. Int. J. of Solids and Structures 38, 4879-4899, 2001.

[9]   Luding, S., Lätzel, M., Volk, W., Diebels, S., Herrmann, H.J.: From discrete element simulations to a continuum model, Comp. Meth. Appl. Mech. Engng. 191, 21-28, 2001.

[10] Tykhoniuk, R., Luding, S., Tomas, J., Simulation der Scherdynamik Kohäsiver Pulver, Chemie Ingenieur Technik 2004, 76, No. 1-2, 59-62.

[11] Deresiewicz, H.: Mechanics of granular matter, Advances in Appl . Mech. 5, 233-306, 1958.

[12] Kappl, M., Butt, H.-J.: The Colloidal Probe Technique and its Application to Adhesion Force Measurements, Part. Part. Syst. Charact. 19, 129-143, 2002.

[13] B.V. Derjaguin, I.I. Abrikosova and E.M. Lifshitz, Quart. Rev. Chem. Soc. 10, 295-329 (1956)

[14] R.S. Bradley, Phil. Mag. 13, 853-862 (1932)

[15] J. Tejchman and W. Wu, Numerical study on patterning of shear bands in a Cosserat continuum, Acta Mechanica 99: 61-74,1993.

[16] G. Hüttl, D. Beyer, E. Müller: Investigation of electrical double layers on SiO_2 surfaces by means of force vs. distance measurements. Surf. Interface Anal. 25 (1997) 543-547.

[17] W.A. Ducker, T. J. Senden, R. M. Pashley: Direct measurement of colloidal forces using an atomic force microscope. Nature 353 (1991) 239-241.

[18] W.A. Ducker, T. J. Senden, R. M. Pashley: Measurement of forces in liquid using a force microscope. Langmuir 8 (1992) 1831-1836.

[19] H.-J. Butt: Measuring electrostatic, van der Waals, and hydration forces in electrolyte solutions with an atomic force microscope. Biophys. J. 60 (1991) 1438-1444.

[20] H.-J. Butt, M. Jaschke, W.A. Ducker: Measuring surface forcesin aqueouss olution with the atomic force microscope. Bioelectrochem. Bioenerg. 381 (1995) 91 - 201.

[21] B. Capella, G. Dietler: Force-distance curves by atomic force microscopy. Surf. Sci. Reports 34 (1999) 1 - 104.